Research Article

Electroless Nickel Deposition: An Alternative for Graphene Contacting

Sinziana M. Popescu,[*,†] Anders J. Barlow,[‡] Sami Ramadan,[§] Srinivas Ganti,[§] Biswajit Ghosh,[‖] and John Hedley[†]
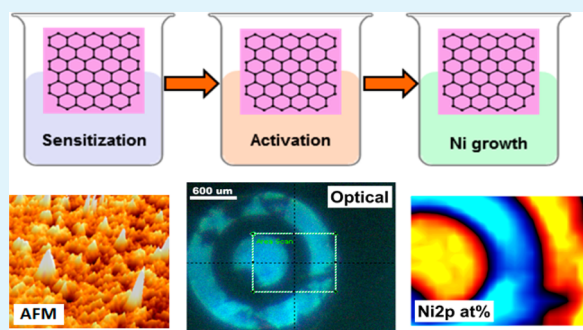
[†]School of Mechanical and Systems Engineering, [‡]National EPSRC XPS Users' Service (NEXUS), and [§]School of Electrical and Electronics Engineering, Newcastle University, NE1 7RU, Newcastle upon Tyne, United Kingdom
[‖]School of Energy Studies, Jadavpur University, Kolkata 700 032, India

S *Supporting Information*

ABSTRACT: We report the first investigation into the potential of electroless nickel deposition to form ohmic contacts on single layer graphene. To minimize the contact resistance on graphene, a statistical model was used to improve metal purity, surface roughness, and coverage of the deposited film by controlling the nickel bath parameters (pH and temperature). The metalized graphene layers were patterned using photolithography and contacts deposited at temperatures as low as 60 °C. The contact resistance was 215 ± 23 Ω over a contact area of 200 $\mu m \times 200$ μm, which improved upon rapid annealing to 107 ± 9 Ω. This method shows promise toward low-cost and large-scale graphene integration into functional devices such as flexible sensors and printed electronics.

KEYWORDS: *contacting graphene, electroless nickel, contact resistance, transmission line method, interface characterization*

INTRODUCTION

Novel nanomaterials such as graphene pose a challenge for available ohmic contact deposition techniques, as the associated contact resistance represents a major drawback in high-performance electronics applications.[1] Different methods have been employed in order to reduce and control contact resistance on graphene, such as improved surface cleanliness,[2] controlled introduction of graphene edges,[3,4] and high purity controlled metal deposition.[5] Contact arrangement and interface engineering have also been attempted for graphene–metal interface improvement.[6,7] Contact resistances on graphene have previously been reported in the range 294 $\Omega \cdot \mu m$[8] to 12 $k\Omega \cdot \mu m$[7] using conventional (thermal and e-beam) evaporation techniques. The reproducibility of contacting methods onto various types of graphene is acknowledged as a major challenge.[9,10]

The electroless nickel plating method provides opportunities over conventional evaporation approaches, the foremost being the processing time (of the order of a few minutes), cost, and accessibility, as it does not require the clean room infrastructure normally associated with evaporation techniques. It can be achieved at low temperatures ($T < 100$ °C), is scalable and ensures isotropic coverage, being suitable for 3D geometries. The method has mainly been applied in printed circuit board manufacture, coatings, and composite applications[11−13] with literature on contact deposition via electroless nickel being limited.[14−17]

With the anticipation of a new generation of devices based on graphene and the advent of a wide range of graphene composites, the development of techniques to make effective contacts to graphene and associated materials is essential. Our group has previously demonstrated the possibility of applying the electroless coating technique onto graphene substrates.[18] The work reported here looks to extend these initial trials on electroless nickel coating onto graphene by forming lithographically patterned ohmic contacts onto transferred CVD graphene substrates. First, we look into photolithography integration for repeatable contact metallization, followed by statistical determination of appropriate pH and temperature of the nickel metallization bath. Finally, a detailed analysis of the nickel–graphene contact resistance is undertaken and the interfacial properties of the coating with graphene are assessed. To our knowledge, this is the first such report on applying and characterizing electroless nickel deposition onto graphene surfaces.

CONTACT FORMATION

Electroless plating is an autonomous, self-catalytic process based on the reduction of metallic ions from an aqueous metal salt-based solution using, for example, a hypophosphite:[19]
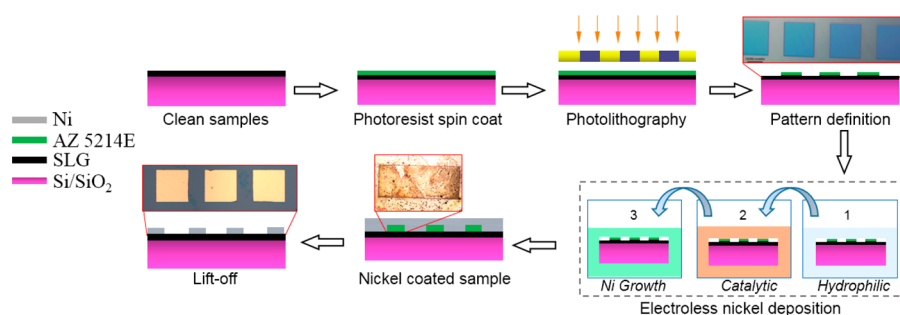
Figure 1. Step-by-step electroless nickel deposition onto CVD graphene substrates: surface cleaning, mask definition via lithography, electroless nickel deposition, and pattern transfer via lift-off technique. Microscope images at ×100 magnification are shown for patterning, nickel deposition, and lift-off steps.
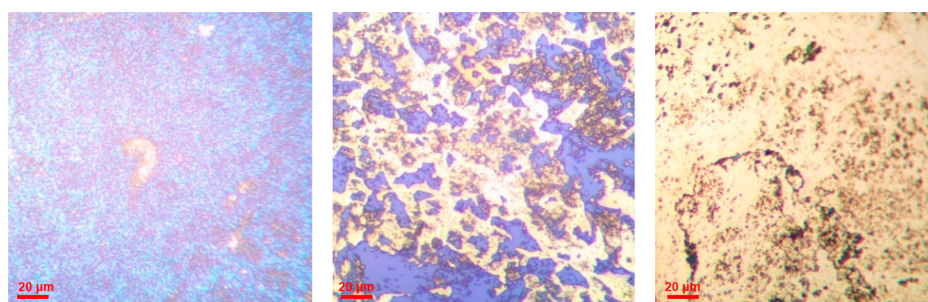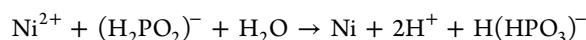

Figure 2. Optical microscope images at successive growth stages of electroless nickel growth on CVD graphene, ×100 magnification. Figure S2 (Supporting Information) shows representative AFM images of growth process.

$$Ni^{2+} + (H_2PO_2)^- + H_2O \rightarrow Ni + 2H^+ + H(HPO_3)^-$$

In electroless nickel plating, once the nickel deposition is initiated, each deposited metal layer acts as a catalytic base, enabling further growth for thicker and more coherent coatings[20] compared to its electrochemical counterpart. The general electroless metallization process includes multiple steps, involving surface cleaning/etching followed by one- or two-step surface activation using tin−palladium based solutions and finally nickel deposition.[20,21] The tin−palladium seeds act as a substrate catalyst, initiating metal deposition. The main advantages of the electroless nickel plating are its tunability and compatibility with a variety of substrates. As with any chemical process, the efficiency of the electroless nickel plating is determined by the experimental conditions employed. The plating rate and metal coating purity are highly dependent on the pH and temperature of the nickel bath[22] but also on the ratio of the concentrations of the reducing agent (e.g., phosphorus, boron, or hydrazine[23]) and the metal salt (e.g., nickel sulfate, nickel chloride[23]). The electroless decoration of plastic with nickel has been achieved at 30−40 °C in an alkaline nickel chloride bath,[24] on carbon nanotubes at 80 °C[25] and 25 °C,[26] carbon nanofibers at 70−90 °C,[27] and glass at temperatures over 85 °C.[28]

A series of experiments were initially performed on unpatterned CVD graphene substrates to identify the optimal sensitization and activation times. In order to study the electrical and interfacial properties, electrodes were defined using photolithography. After an initial mask definition, lift-off could be performed at either activation or deposition stages. When performed after activation, the tin/palladium molecular layer was partially removed in acetone, hence inhibiting further nickel deposition in the final step. When performed after metallization, the nickel deposition showed more consistency

but issues of adhesion persisted, with process parameters requiring optimization. The integration of electroless nickel plating was finally integrated with mask definition, as depicted in Figure 1, with details provided in Methods.

The patterned graphene "windows" were inspected throughout the process in order to confirm the preparation of the graphene surface for nickel deposition. Colloidal particles were visible under the optical microscope after the sensitization step, presenting a uniform coating of tin chloride. For activation, XPS analysis confirmed the chemisorption of palladium catalytic molecules onto the sensitized graphene surface (Figure S1 in Supporting Information). To determine suitable plating parameters, the graphene samples were metallized in various conditions of the nickel electroless bath according to a basic statistical model, using the most and least extreme pH and temperature conditions in the chosen range (i.e., 60−90 °C, pH 6−8). This range was chosen based on previously reported literature of nickel electroless plating,[21,25,27,29,30] a summary of which is given in Table S1. A continuous nickel film was observed over the entire surface prior to the lift-off step for all samples. Figure 2 shows the graphene−nickel surface at different growth stages, evolving from discrete particles into islands and finally coalescence of the islands. AFM images of the electroless nickel growth process are shown in Figure S2. Once the coalescence point was reached, the growth rate of the Ni−P film became linear, in agreement with literature.[31] For MEMS applications, the thickness of the deposited layer must be controllable, which is achievable based on the linear characteristic of the electroless process once the nickel film continuity is achieved. The growth/deposition rate is highly sensitive to the electroless nickel bath conditions.

EDX analysis was performed on continuous nickel films at different deposition times, as shown in Table 1. As removal of the sample would require reactivation (PdCl₂ immersion)

Table 1. EDX-Determined Ni:P Film Composition as Function of Electroless Deposition Time

time [s]	Ni [at %]	P [at %]	Si/C/O [at %]
60	43	8.8	47.2
90	44	8.9	46.5
120	58	9.6	32.2
160	79.7	15.4	4.4

before further plating, which would introduce variability in terms of Ni−P composition, different samples were interrupted during the electroless metallization process. Results indicated that with increasing deposition time and film thickness, the Ni:P ratio stabilizes and a better coverage is obtained.

Thicker nickel deposits are observed at the edges of the contacts, indicative of the favored electroless coating at the lithographically defined edges. This may be facilitated by the hydrophilicity of the photoresist. The nickel contacts obtained upon lift-off are shown in Figure 3, each image being
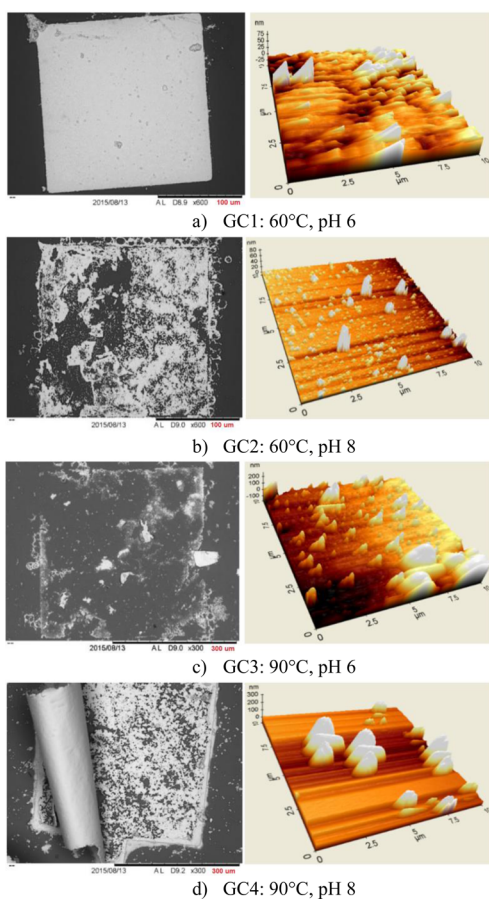

Figure 3. Nickel electroless deposition on CVD graphene in conditions of varied bath parameters (temperature °C, pH) marked as GC1−GC4: SEM (left) and 3D AFM (right) images (10 μm × 10 μm) of the contacts.

representative of contact definition at the specified temperature and pH conditions: GC1 and GC2 at 60 °C and pH 6 and 8, respectively, and GC3 and GC4 at 90 °C and pH 6 and 8, respectively. Comparative Ni 2p XPS spectra of the four samples are included in Figure S3. Under all conditions tested except for GC1, the nickel layer exhibited poor adhesion to the sample, while GC2 and GC3 conditions resulted in discontinuous coating. The deposited nickel films tended to peel to form scrolls in GC4 conditions.

The contact resistance depends on the metallic film's electrical resistivity and interfacial properties. As the electroless deposited film is a Ni−P alloy, the bulk resistivity varies with the P content.[32] It is also acknowledged that the electronic properties of electro(less)-deposited nickel are different from pure Ni.[23] The increase of P content reduces the density of states at Fermi level, resulting in an increase in the work function of Ni−P.[33] By improving the morphology of the electroless nickel film, one can further decrease the contact resistance. Xia et al.[1] showed that a smooth metal surface reduces scattering and increases the mean free path, improving the graphene−metal contact.

Therefore, high nickel metal purity, good interface adhesion, and low surface roughness are essential for obtaining low contact resistance on CVD graphene. EDX and AFM measurements were used to quantify the atomic concentrations, coverage, and surface roughness and are presented in Table 2. In the case of poorly adhered contacts, nickel flakes were selected for the analysis.

The obtained contour plots presented in Figure 4 indicate that the metallic purity of the coating is highly dependent on the pH of the electroless nickel bath, showing a Pearson correlation coefficient of −0.897, with very limited temperature sensitivity. On the other hand, the surface roughness exhibits an opposite trend with a Pearson coefficient of 0.669 for temperature. A customized multiple response surface design was used to determine that 66 °C and pH 6.6 were suitable bath parameters for the electroless nickel process.

■ ELECTRICAL PROPERTIES

The contact resistance was extracted via transfer length method (TLM) structures[34] with both linear (LTLM) and circular (CTLM) patterns defined. The electroless nickel bath was controlled at a temperature of 66 ± 1 °C and pH of 6.6 ± 0.1 with a nickel deposition time under 4 min.

Poor adhesion of the nickel film on the samples was still observed in certain areas under these chosen bath conditions, with a deposited layer thickness of between 400 and 700 nm. The local differences in nickel film height can be explained due to the growth being island based. In addition, graphene is known to be highly hydrophobic[35] and one can expect faster nickel deposition rates on the photoresist and graphene defective areas which have improved chemical wettability.[36]

Rapid annealing experiments on graphene contacts have demonstrated residue elimination, improved surface smooth-

Table 2. Surface Characteristics of the Electroless Process at Various Temperatures and pH

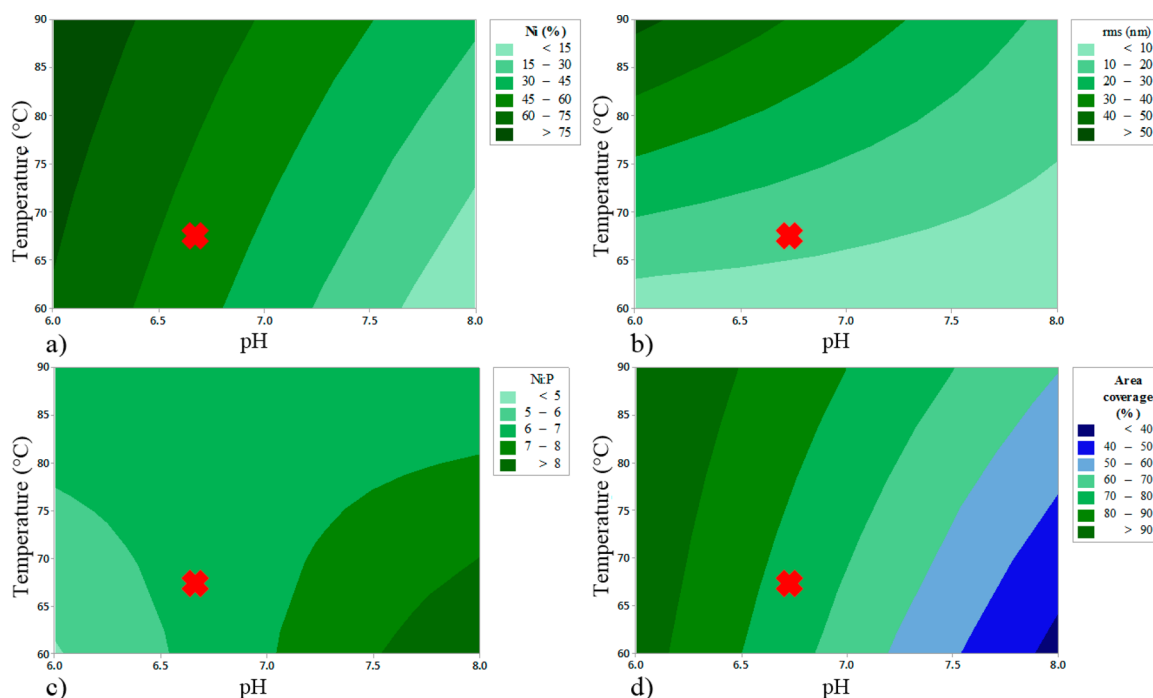| temp [°C]	pH	Ni [at %]	P [at %]	Ni:P	C [at %]	Si [at %]	O$_2$ [at %]	rms [nm]	coverage [%]
60	6.0	73.5	14.9	4.9	3.3	5.6	2.4	5.1	94.4
60	8.0	2.6	0.3	8.9	0	63.2	33.9	2.3	36.8
90	6.0	85.4	12.6	6.8	0	0.5	0.1	52.5	99.5
90	8.0	32.2	5.2	6.2	8.2	39.6	14.8	17.5	60.5

Figure 4. Contour plots showing the effect of pH and temperature on (a) nickel purity, (b) surface roughness, (c) Ni:P ratio, (d) nickel coverage. Statistically determined graphene-suitable bath parameters are marked with a red cross.

ness[37] and enhancement of the interface due to the formation of strong covalent bonds between the nickel surface and graphene layer.[38] We performed rapid annealing on the samples at 400 °C (120 s) to assess any improvement of the graphene–nickel interface.

The LTLM contacts demonstrated a more consistent adhesion and were thus used for electrical characterization. The I–V contact characteristics, an example of which is shown in Figure 5, confirm the ohmic nature of the contact. After
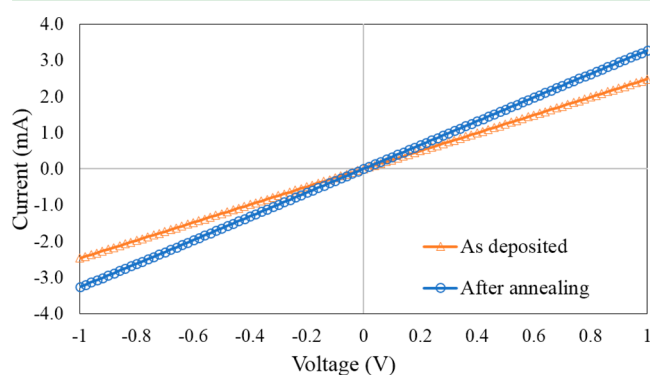

Figure 5. A representative I–V characteristic curve for two adjacent contacts before and after annealing.

annealing, the total resistance decreased by 32% (average). Assuming a uniform sheet resistance, the total measured resistance as a function of intercontact length l is defined by

$$R_{\mathrm{T}} = \frac{R_{\mathrm{sh}}}{W}l + 2R_{\mathrm{C}} \qquad (1)$$

where R_{sh}, R_{C}, and W are the sheet resistance of the graphene, contact resistance, and contact width, respectively. The contact resistance is determined from a linear fit of the measurements from each of the samples (S1–S4) as deposited and after the

annealing treatment, being shown in Figure 6. The extrapolated contact resistance (Ω) is converted into $R_{\mathrm{C}}W$ units for a more suitable expression and interpretation.[39] The average contact resistance of $215 \pm 23\ \Omega$ for as-deposited samples corresponds to $43 \pm 5\ \mathrm{k\Omega\cdot\mu m}$, and it is significantly reduced by 50% to $107 \pm 9\ \Omega$ ($21 \pm 2\ \mathrm{k\Omega\cdot\mu m}$) after the annealing treatment. It is observed that the annealing treatment improves the adhesion of the nickel onto the samples, in agreement with Gahoi et al.,[40] but it ultimately affects the morphology of the nickel layer as circular blisters are formed, especially on the poorly adhered regions (inset in Figure 6). This can be explained by the presence of air/gas bubbles which are common in thin metal layers.[41,42]

ASSESSMENT OF FILM QUALITY AND INTERFACE TO GRAPHENE

The postdeposition annealing treatment at temperatures of 300–600 °C facilitates the crystallization process, leading to an increase in the average grain size and surface roughness.[19] Microcrystalline nickel and nickel phosphide (Ni_3P) are the common phases for the annealed metal-based composite film and can lead to some level of P atom diffusion.[43] Surface analysis was performed in order to investigate these aspects.

EDX showed that the P content decreased from 14% to 5% on average as a result of the annealing treatment. AFM and ESEM (Figure S4) confirmed an increase in Ni–P film surface roughness from 1 to 42 nm after annealing with the grain size for the annealed sample being 900 nm on average. XRD measurements (Figure S5) show a sharp peak at 44.5° indicating (111) orientation. The annealing process drives the initially seeded crystal to further crystallization reflected by 2 orders of magnitude increase in the peak intensity. The (111) arrangement is most prevalent, since it offers the closest packing in the lattice structure for an FCC unit cell with minimum interplanar spacing ($d = 2.035$ Å).[44] This suggests a reduced bulk resistivity of the annealed Ni–P films due to
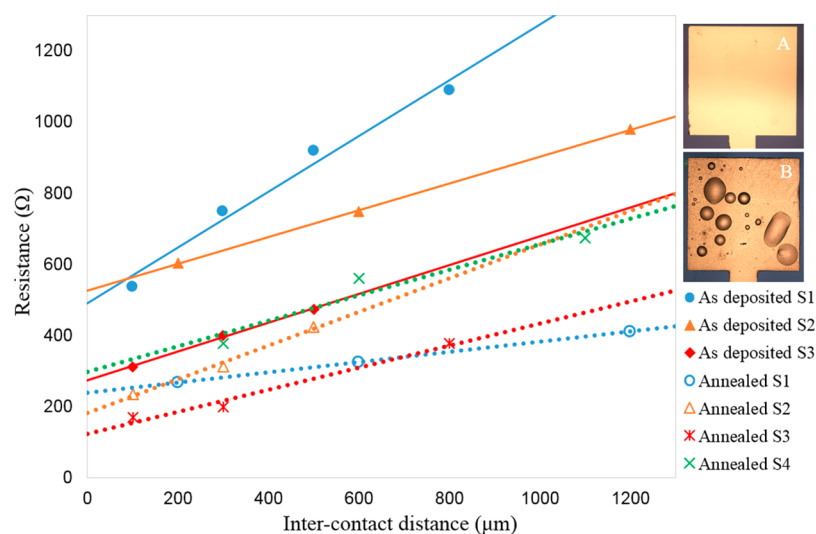
Figure 6. Resistance measurements for increasing intercontact distances for electroless nickel on graphene. R_C is determined as half of the Y-axis intercept. Inset: optical microscope image at ×200 magnification: contact before annealing (A) and after annealing (B).
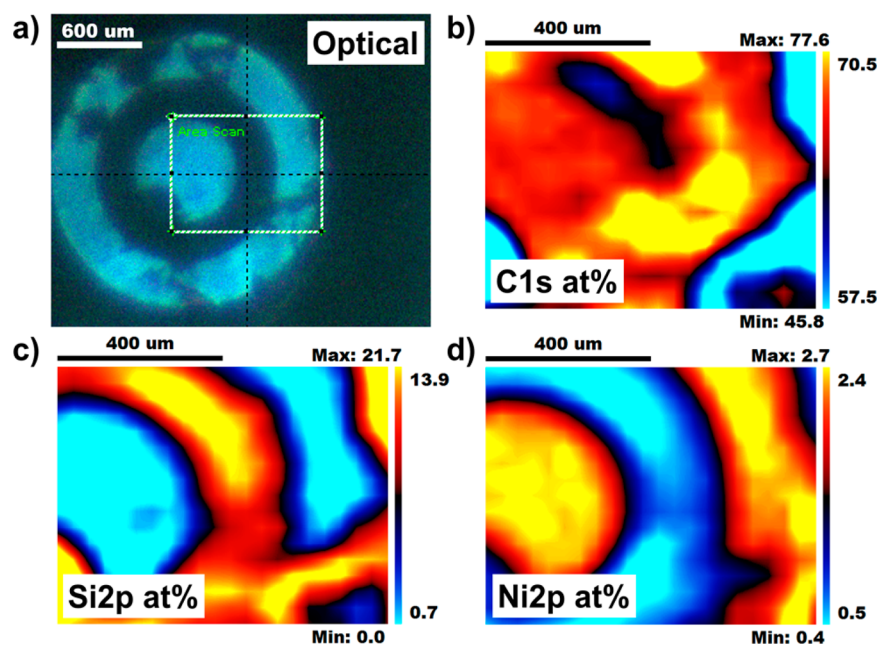

Figure 7. XPS maps of a patterned electroless nickel coated graphene structure: (a) optical image of the mapped area; data for (b) carbon, (c) silicon, (d) nickel. Intensity given as quantified atomic percentages.

larger, preferentially oriented grains (less electron scattering), as opposed to the more randomly oriented grains in the as-grown films.

Gaps and poorly adhered areas in the nickel-defined contacts were investigated using XPS and Raman characterization techniques. Figure 7 presents results from XPS mapping of a CTLM structure. The region under analysis is shown in Figure 7a as obtained from the instrument's microscope, where the mapped region is indicated by the green box. Quantified (atomic %) XPS maps for carbon, silicon, and nickel are presented in Figure 7b−d, respectively. The strong silicon signal in areas with visible delamination of the nickel layer is indicative of the graphene layer delaminating from the silicon substrate during the patterning process. This is further confirmed by XPS carbon C 1s spectra, where in regions of

delamination, little carbon is present. The complete XPS survey is included in Figure S6.

Raman spectra was taken across two areas of interest, one being protected by the photoresist during plating (denoted as A) and the other where the plated nickel has delaminated (denoted as B, regions shown in Figure S7). The variation of graphene quality across area A is substantial, with single ($I_{2D}/I_G \approx 1.35$) and bilayer ($I_{2D}/I_G \approx 0.55$) graphene present but also gaps are present in the graphene layer, exposing the silicon dioxide substrate. With two interfaces being involved in graphene contacting applications, graphene−substrate and graphene−metal,[45,46] graphene quality and uniformity play a major role in interface performance. Asadi et al.[47] named common issues associated with transferred CVD graphene, the most crucial of which here is that the graphene is prone to edge cracks and associated discontinuities which degrade further
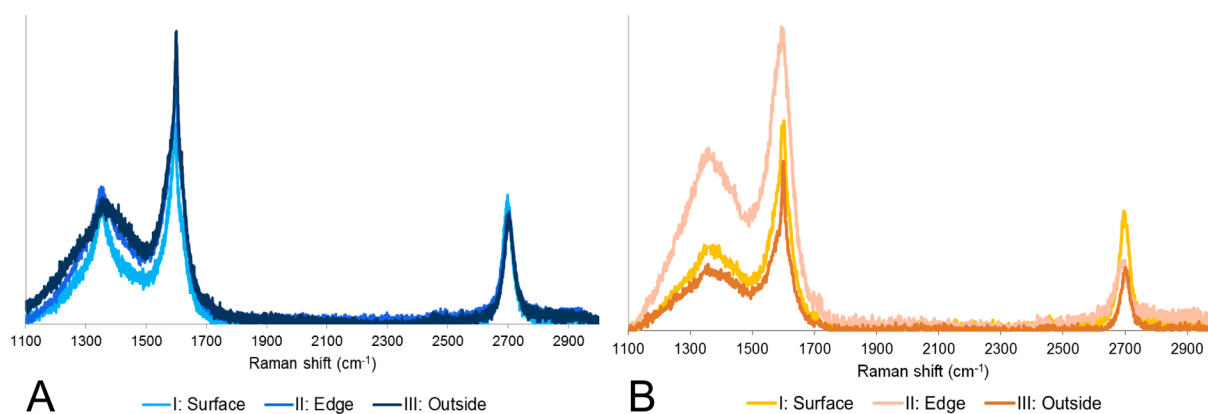
Figure 8. Representative Raman of graphene after the etching of (top image) as-deposited electroless nickel and (bottom image) annealed electroless nickel in different areas of the patterned samples.
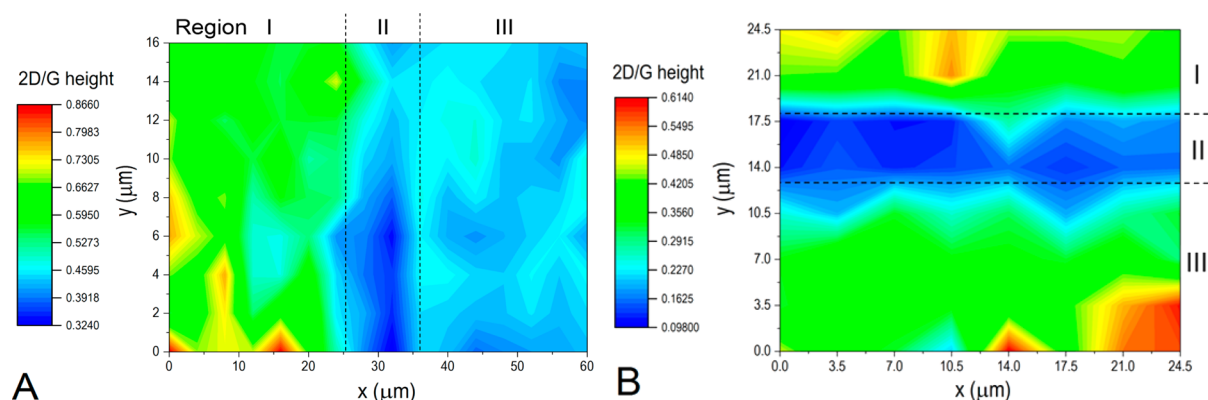

Figure 9. Raman mapping study of nickel−graphene interface, after nickel etching of (a) as-deposited and (b) annealed graphene. Regions represent the following: (I) contact surface, (II) edge of the contact, (III) outside contacts.

upon photoresist patterning. The mild cleaning process also affects the quality of the graphene layer, with marked increase in the Raman peak intensity ratio I_D/I_G from 0.3 for noncleaned graphene to 0.4 for cleaned graphene and a decrease in I_{2D}/I_G from 4.3 to 0.6 (Figure S8). This aspect was also reflected in graphene sheet resistance which increased from an average of 350 Ω/sq to 700 Ω/sq (three samples measured). The Raman peak intensity ratio changes are representative of bilayer graphene being formed[48] due to folds and creases in the initial single layer graphene. The sheet resistance measurements further indicate gaps and interruptions in the graphene layer. In poorly adhered graphene regions, although these would be nickel plated, subsequent delamination of the graphene also removed the nickel coating, evident from the sparsity of graphene in regions where the nickel plating was unsuccessful.

For further study of the graphene−nickel interface, the electroless deposited nickel film was etched by a method similar to that of Leong et al.[38] Figure 8 illustrates representative Raman maps after the electroless deposited nickel etching for the as-deposited and annealed patterned graphene samples in three regions: inside (location of the nickel-based film), edge (of deposited film), and outside contacts. The broadened D ($\sim$1360 cm^{-1}) and G ($\sim$1590 cm^{-1}) peaks are characteristic for functionalized graphene,[49] while the present, well-defined 2D peak at $\sim$2700 cm^{-1} confirms the presence of single-layer graphene. A further broadening of the D (by $\sim$75 cm^{-1}) and G peaks (by $\sim$170 cm^{-1}) at the electroless nickel contact edge for the annealed sample confirms a higher defect density in this region. As Cançado et al.[50] have discussed, there are fine differences between "silent" and structural defects in graphene. However, in our case the D peak is not dominating the Raman spectra, indicating that the electroless-activated single-layer graphene is not significantly structurally disordered.[51]

Raman maps of the graphene−nickel interface also reveal some distinctive trends, presented in Figure 9. The 2D:G intensity ratio shows a decrease from 0.61 to 0.43 over the etched nickel regions suggesting increased defects/doping in this region after annealing. This compares with a 0.44−0.40 ratio change in the exposed graphene regions outside of the contacts. However, the contact edge graphene−nickel interface exhibits significant changes as a result of the heat treatment, the ratio changing from 0.45 to 0.18. This marked difference in ratio at the edge is believed to be due to the favored growth toward the hydrophilic photoresist regions leading to a higher dopant concentration in the graphene, changing the interface properties.[52] The significant reduction in contact resistance after the annealing treatment can be explained by the enhanced chemical reactivity of graphene via carbon dangling bonds[53] combined with some level of Ni doping.[54]

When this contact fabrication approach is compared to other reported techniques, lower contact resistances are currently obtained from evaporation approaches. Options to reduce this electroless nickel contact resistance are work function engineering by the electroless deposition of metal combinations[22,55] or graphene doping,[56] and our work provides a useful basis for further investigation in this area.

CONCLUSIONS

Electroless nickel deposition was explored for the first time as a metallization alternative for CVD transferred single-layer graphene substrates. The obtained average nickel contact resistance of 43 ± 5 kΩ·μm significantly improved via annealing at 400 °C giving a 50% reduction in contact resistance to 21 ± 2 kΩ·μm. Surface analysis indicated that variable metal adhesion onto the graphene samples is a side effect of discontinuities in the CVD transferred graphene due to cleaning and lithography process steps. Examination of the interface suggests further crystallization of the nickel and enhancement of the Ni−C bonding is achieved upon annealing. Intrinsic stresses are formed in the nickel film due to the deposition process, including hydrogen desorption and growth of islands, while extrinsic stresses emerge due to different thermal properties between the film and substrate during removal of the sample from the nickel bath and subsequent cooling. A good graphene−substrate interface should be ensured prior to any experimental work for minimizing delamination due to Ni−P film stresses. Further work should target the compatibility of photolithography with electroless deposition techniques with careful optimization of film uniformity (controlled growth), slow substrate cooling after the electroless deposition process, and the annealing temperature.

The method is expected to be transferable to various graphene-based materials, but as the electroless plating bath parameters are highly dependent on the properties of the substrate to be coated, bath parameters may require tuning for these materials. It is anticipated that through work function engineering, this simple, low-temperature metallization method can ultimately be developed for integration with graphene based electronic technologies and is worthy of further investigation.

METHODS

Graphene samples were purchased from Graphenea (Spain) and consisted of single-layer graphene transferred onto a 4 in. SiO_2/Si substrate wafer and then diced into 7 mm × 7 mm squares. Chemicals were purchased from Sigma-Aldrich (U.K.) unless otherwise stated.

Cleaning Method. The graphene samples were cleaned by rinsing in acetone and isopropanol and blow dried with a nitrogen gun. UV lithography (Karl Suss MJB-3) was performed to define the contacts, selectively exposing the graphene areas. The LTLM mask consisted of sets of pads at distances varying between 50 and 400 μm for consecutive electrodes. The CTLM mask contained concentric patterns with radii between 100 and 1000 μm.

Electroless Nickel Deposition and Etching. The patterned graphene samples were immersed in a tin sensitizing solution (80 g/L tin(II) chloride with 37% hydrochloric acid in deionized water, solution 1 in Figure 2) at room temperature for 3 min. After a single rinsing step in deionized water, the samples were immersed in a 50 °C heated activating solution (0.15 g/L palladium chloride in deionized water, solution 2 in Figure 1) for 5 min. Upon activation, the samples were rinsed twice in deionized water and then placed in the nickel plating bath (solution 3 of Figure 1) for 4 min. The electroless nickel plating bath, adapted from a previous study,[18] was prepared from two initial aqueous solutions heated to 50 °C prior to mixture: a metal-based solution containing nickel sulfate (35 g/L) with ammonium chloride (50 g/L) and a reducing agent-based solution containing sodium hypophosphite (15 g/L) with sodium citrate (50 g/L). Different bath conditions were tested with pH adjustment (6−8) being controlled by addition of ammonium hydroxide and a hot plate used for temperature control (60−90 °C). Upon removal from the nickel-based bath, the samples have been rinsed with DI water held at a temperature of approximately 35 °C and placed in the oven at 50 °C for 15 min in order to facilitate the surface drying. The selectively deposited nickel contacts were released via a final lift-off step in acetone. The postmetallization annealing was performed in an RTP (JetFirst 200) furnace in forming gas $N_2:H_2$ (97:3) for 120 s.

The nickel film was etched by sample immersion in 70 °C heated aqua regia for less than 1 min. The acid solution was obtained by mixing 69.5% nitric acid (Technic) and 37% concentrated hydrochloric acid (Technica) in 1:3 ratio.

Measurements and Analysis. The photoresist step and nickel contact height upon lift-off were checked using a Tencor P-1 long scan profiler. Nickel−graphene surface analysis and imaging were performed using X-ray photoelectron spectroscopy (K-Alpha XPS, Thermo Scientific, East Grinstead), atomic force microscopy (XE-150, Park Systems), Raman spectroscopy (Horiba Jobin Yvon LabRAM HR800), and scanning electron/energy dispersive microscopy (SEM-EDX, Hitachi TM3030). The electrical measurements were taken using an Agilent B1500 system.

The Raman maps were batch processed to obtain reasonable fits to the data, using Lorentzian peaks at the expected D, G, and 2D positions. Contour profile plots are presented to visualize the variation of the relevant peak ratios. High-resolution ESEM images were obtained using XL30 ESEM system at the Electron Microscopy Unit, Newcastle University.

XRD measurements were performed using a Bruker D8 ADVANCE instrument with Cu source (λ = 0.154 nm), using a simple $\theta/(2\theta)$ setup. True parallel beam conditions were achieved by using a Göebel mirror and axial Soller at the source and detector, respectively. Line broadening effects are minimal at the relatively low angles of interest in this study and, as such, are neglected.

ASSOCIATED CONTENT

Ⓢ Supporting Information

The Supporting Information is available free of charge on the ACS Publications website at DOI: 10.1021/acsami.6b08290.

> XPS spectra for the assessed pH−temperature parameters; AFM images of growth process; XRD and ESEM before and after annealing; XPS surveys and Raman spectra for patterned graphene−nickel structures; Raman spectra and optical images for CVD single-layer graphene before and after cleaning procedures (PDF)

AUTHOR INFORMATION

Corresponding Author

*E-mail: s.m.popescu@newcastle.ac.uk.

Notes

The authors declare no competing financial interest.

ACKNOWLEDGMENTS

■ REFERENCES

(1) Xia, F.; Perebeinos, V.; Lin, Y.; Wu, Y.; Avouris, P. The Origins and Limits of Metal−graphene Junction Resistance. *Nat. Nanotechnol.* **2011**, 6 (3), 179−184.

(2) Gahng, S.; Ho Ra, C.; Jin Cho, Y.; Ah Kim, J.; Kim, T.; Jong Yoo, W. Reduction of Metal Contact Resistance of Graphene Devices via CO2 Cluster Cleaning. *Appl. Phys. Lett.* **2014**, 104 (22), 223110.

(3) Smith, J. T.; Franklin, A. D.; Farmer, D. B.; Dimitrakopoulos, C. D. Reducing Contact Resistance in Graphene Devices through Contact Area Patterning. *ACS Nano* **2013**, 7 (4), 3661−3667.

(4) Chu, T.; Chen, Z. Understanding the Electrical Impact of Edge Contacts in Few-Layer Graphene. *ACS Nano* **2014**, 8 (4), 3584−3589.

(5) Zhong, H.; Zhang, Z.; Chen, B.; Xu, H.; Yu, D.; Huang, L.; Peng, L. Realization of Low Contact Resistance close to Theoretical Limit in Graphene Transistors. *Nano Res.* **2015**, 8 (5), 1669−1679.

(6) Park, H.-Y.; Jung, W.-S.; Kang, D.-H.; Jeon, J.; Yoo, G.; Park, Y.; Lee, J.; Jang, Y. H.; Lee, J.; Park, S.; Yu, H.-Y.; Shin, B.; Lee, S.; Park, J.-H. Graphene: Extremely Low Contact Resistance on Graphene through N-Type Doping and Edge Contact Design (Adv. Mater. 5/2016). *Adv. Mater.* **2016**, 28 (5), 975−975.

(7) Krishna Bharadwaj, B.; Nath, D.; Pratap, R.; Raghavan, S. Making Consistent Contacts to Graphene: Effect of Architecture and Growth Induced Defects. *Nanotechnology* **2016**, 27 (20), 205705.

(8) Leong, W. S.; Gong, H.; Thong, J. T. L. Low-Contact-Resistance Graphene Devices with Nickel-Etched-Graphene Contacts. *ACS Nano* **2014**, 8 (1), 994−1001.

(9) Russo, S.; Craciun, M. F.; Yamamoto, M.; Morpurgo, A. F.; Tarucha, S. Contact Resistance in Graphene-Based Devices. *Phys. E* **2010**, 42 (4), 677−679.

(10) Hsu, A.; Wang, H.; Kim, K. K.; Kong, J.; Palacios, T. Impact of Graphene Interface Quality on Contact Resistance and RF Device Performance. *IEEE Electron Device Lett.* **2011**, 32 (8), 1008−1010.

(11) Hardinnawirda, K.; Zetty Akhtar, A. M.; Aisha, I. S. R.; Mahadzir, I. Deposition of Electroless Nickel Boron as Printed Circuit Board Surface Finish. *Adv. Mater. Res.* **2016**, 1133, 391−395.

(12) Alishahi, M.; Monirvaghefi, S. M.; Saatchi, A.; Hosseini, S. M. The Effect of Carbon Nanotubes on the Corrosion and Tribological Behavior of Electroless Ni−P−CNT Composite Coating. *Appl. Surf. Sci.* **2012**, 258 (7), 2439−2446.

(13) Sudagar, J.; Lian, J.; Sha, W. Electroless Nickel, Alloy, Composite and Nano Coatings − A Critical Review. *J. Alloys Compd.* **2013**, 571, 183−204.

(14) Sullivan, M. V.; Eigler, J. H. Electroless Nickel Plating for Making Ohmic Contacts to Silicon. *J. Electrochem. Soc.* **1957**, 104 (4), 226.

(15) Kanungo, J.; Pramanik, C.; Bandopadhyay, S.; Gangopadhyay, U.; Das, L.; Saha, H.; Gettens, R. T. T. Improved Contacts on a Porous Silicon Layer by Electroless Nickel Plating and Copper Thickening. *Semicond. Sci. Technol.* **2006**, 21 (7), 964.

(16) Rohan, J. F.; O'Riordan, G.; Boardman, J. Selective Electroless Nickel Deposition on Copper as a Final Barrier/bonding Layer Material for Microelectronics Applications. *Appl. Surf. Sci.* **2002**, 185 (3–4), 289−297.

(17) RAVAL, M. C.; SOLANKI, C. S. Characterization of Electroless Nickel as a Seed Layer for Silicon Solar Cell Metallization. *Bull. Mater. Sci.* **2015**, 38 (1), 197−201.

(18) Ghosh, B.; Dale, C.; Dewanto, R.; Keegan, N.; Hedley, J. A Novel Electrical Contacting Technology To Graphene. *Nanotechnology* **2012**, 1, 196−199.

(19) Mallory, G. O.; Hajdu, J. B. *Electroless Plating: Fundamentals and Applications*; William Andrew Publishing/Noyes: New York, 1990.

(20) Sahoo, P.; Das, S. K. Tribology of Electroless Nickel Coatings - A Review. *Mater. Eng.* **2011**, 32 (4), 1760−1775.

(21) Schlesinger, M. Electroless Deposition of Nickel. In *Modern Electroplating*; John Wiley & Sons, Inc.: Hoboken, NJ, 2010; pp 447−458.

(22) Ghosh, B. Electrical Contacts for II−VI Semiconducting Devices. *Microelectron. Eng.* **2009**, 86 (11), 2187−2206.

(23) Kundu, S.; Das, S. K.; Sahoo, P. Properties of Electroless Nickel at Elevated Temperature - A Review. *Procedia Eng.* **2014**, 97, 1698−1706.

(24) Dennis, J. K.; Such, T. E. *Nickel and Chromium Plating*, 3rd ed.; Woodhead Publishing Limited: Cambridge, U.K., 1993.

(25) Liebau, M.; Unger, E.; Duesberg, G. S.; Graham, A. P.; Seidel, R.; Kreupl, F.; Hoenlein, W. Contact Improvement of Carbon Nanotubes via Electroless Nickel Deposition. *Appl. Phys. A: Mater. Sci. Process.* **2003**, 77 (6), 731−734.

(26) Ang, L. M.; Hor, T. S. A.; Xu, G. Q.; Tung, C. H.; Zhao, S. P.; Wang, J. L. S. Decoration of Activated Carbon Nanotubes with Copper and Nickel. *Carbon* **2000**, 38 (3), 363−372.

(27) Tzeng, S.-S.; Chang, F.-Y. Electrical Resistivity of Electroless Nickel Coated Carbon Fibers. *Thin Solid Films* **2001**, 388 (1−2), 143−149.

(28) Wei, X.; Roper, D. K. Tin Sensitization for Electroless Plating Review. *J. Electrochem. Soc.* **2014**, 161 (5), D235−D242.

(29) Aleksinas, M. J. Troubleshooting Electroless Nickel Plating Solutions. In *Electroless Plating: Fundmentals and Applications*; William Andrew Publishing/Noyes: Orlando, FL, 1990, Chapter 3, 101−109.

(30) Muraliraja, R.; Elansezhian, R.; Patterson, K. Optimization of Reducing Agent and Key Parameters Effect on the Efficiency of Electroless Ni-P Plating by Taguchi Method. *Procedia Mater. Sci.* **2014**, 5, 2478−2486.

(31) Schlesinger, M. Electroless Deposition of Nickel. In *Modern Electroplating*; John Wiley & Sons, Inc.: Hoboken, NJ, 2011; pp 447−458.

(32) Parkinson, R. *Properties and Applications of Electroless Nickel*; Technical Literature, Nickel Institute: Toronto, Canada, 1995.

(33) Elsener, B.; Crobu, M.; Scorciapino, M. A.; Rossi, A. Electroless Deposited Ni−P Alloys: Corrosion Resistance Mechanism. *J. Appl. Electrochem.* **2008**, 38 (7), 1053−1060.

(34) Deen, M.; Pascal, F. Electrical Characterization of Semiconductor Materials and Devices. *Surv. High Energy Phys.* **2006**, 409−438.

(35) Martins, L. G. P.; Song, Y.; Zeng, T.; Dresselhaus, M. S.; Kong, J.; Araujo, P. T. Direct Transfer of Graphene onto Flexible Substrates. *Proc. Natl. Acad. Sci. U. S. A.* **2013**, 110 (44), 17762−17767.

(36) Li, Z.; Wang, Y.; Kozbial, A.; Shenoy, G.; Zhou, F.; McGinley, R.; Ireland, P.; Morganstein, B.; Kunkel, A.; Surwade, S. P.; Li, L.; Liu, H. Effect of Airborne Contaminants on the Wettability of Supported Graphene and Graphite. *Nat. Mater.* **2013**, 12 (10), 925−931.

(37) Jang, C. W.; Kim, J. H.; Kim, J. M.; Shin, D. H.; Kim, S.; Choi, S.-H. Rapid-Thermal-Annealing Surface Treatment for Restoring the Intrinsic Properties of Graphene Field-Effect Transistors. *Nanotechnology* **2013**, 24 (40), 405301.

(38) Leong, W. S.; Nai, C. T.; Thong, J. T. L. What Does Annealing Do to Metal−Graphene Contacts? *Nano Lett.* **2014**, 14 (7), 3840−3847.

(39) Nagashio, K.; Nishimura, T.; Kita, K.; Toriumi, A. Contact Resistivity and Current Flow Path at Metal/graphene Contact. *Appl. Phys. Lett.* **2010**, 97 (14), 143514.

(40) Gahoi, A.; Wagner, S.; Bablich, A.; Kataria, S.; Passi, V.; Lemme, M. C. Contact Resistance Study of Various Metal Electrodes with CVD Graphene. *Solid-State Electron.* **2016**, 125, 234.

(41) Di Bari, G. A. Electrodeposition of Nickel. In *Modern Electroplating*; John Wiley & Sons, Inc.: Hoboken, NJ, 2011; pp 79−114, DOI: 10.1002/9780470602638.ch3.

(42) Gadkari, P. Effect of Annealing on Copper Thin Films: The Classical Size Effect and Agglomeration. M.Sc. Thesis, University of Central Florida, Orlando, FL, 2005.

(43) Kundu, S.; Das, S. K.; Sahoo, P. Properties of Electroless Nickel at Elevated Temperature-a Review. *Procedia Eng.* **2014**, 97, 1698−1706.

(44) Lee, D. N.; Han, H. N. Recrystallization Textures of Metals and Alloys. In *Recent Developments in the Study of Recrystallization*; InTech: Rijeka, Croatia, 2013; DOI: 10.5772/54123.

(45) Liu, W.; Wei, J.; Sun, X.; Yu, H. A Study on Graphene—Metal Contact. *Crystals* **2013**, 3 (1), 257−274.

(46) Wang, H.; Hsu, A.; Palacios, T. Graphene Electronics for RF Applications. *IEEE Microw. Mag.* **2012**, *13* (4), 114−125.

(47) Asadi, K.; Timmering, E. C.; Geuns, T. C. T.; Pesquera, A.; Centeno, A.; Zurutuza, A.; Klootwijk, J. H.; Blom, P. W. M.; de Leeuw, D. M. Up-Scaling Graphene Electronics by Reproducible Metal−Graphene Contacts. *ACS Appl. Mater. Interfaces* **2015**, *7* (18), 9429−9435.

(48) Calizo, I.; Bejenari, I.; Rahman, M.; Liu, G.; Balandin, A. A. Ultraviolet Raman Microscopy of Single and Multilayer Graphene. *J. Appl. Phys.* **2009**, *106* (4), 43509.

(49) Englert, J. M.; Dotzer, C.; Yang, G.; Schmid, M.; Papp, C.; Gottfried, J. M.; Steinrück, H.-P.; Spiecker, E.; Hauke, F.; Hirsch, A. Covalent Bulk Functionalization of Graphene. *Nat. Chem.* **2011**, *3* (4), 279−286.

(50) Cançado, L. G.; Jorio, A.; Ferreira, E. H. M.; Stavale, F.; Achete, C. A.; Capaz, R. B.; Moutinho, M. V. O.; Lombardo, A.; Kulmala, T. S.; Ferrari, A. C. Quantifying Defects in Graphene via Raman Spectroscopy at Different Excitation Energies. *Nano Lett.* **2011**, *11* (8), 3190−3196.

(51) Gao, G.; Liu, D.; Tang, S.; Huang, C.; He, M.; Guo, Y.; Sun, X.; Gao, B. Heat-Initiated Chemical Functionalization of Graphene. *Sci. Rep.* **2016**, *6*, 20034.

(52) Peng, S.; Jin, Z.; Ma, P.; Zhang, D.; Shi, J.; Niu, J.; Wang, X.; Wang, S.; Li, M.; Liu, X.; Ye, T.; Zhang, Y.; Chen, Z.; Yu, G. The Sheet Resistance of Graphene under Contact and Its Effect on the Derived Specific Contact Resistivity. *Carbon* **2015**, *82*, 500−505.

(53) Ma, B.; Gong, C.; Wen, Y.; Chen, R.; Cho, K.; Shan, B. Modulation of Contact Resistance between Metal and Graphene by Controlling the Graphene Edge, Contact Area, and Point Defects: An Ab Initio Study. *J. Appl. Phys.* **2014**, *115* (18), 183708.

(54) Wang, W. X.; Liang, S. H.; Yu, T.; Li, D. H.; Li, Y. B.; Han, X. F. The Study of Interaction between Graphene and Metals by Raman Spectroscopy. *J. Appl. Phys.* **2011**, *109* (7), 07C501.

(55) Ghosh, B.; Mandal, R. Evaluation of Electrical Contact in Thin Semiconducting Films From AC Measurements. *IEEE J. Electron Devices Soc.* **2016**, *4* (4), 179−184.

(56) Tao, H.-C.; Yang, X.-L.; Zhang, L.-L.; Ni, S.-B. One-Step Synthesis of Nickel sulfide/N-Doped Graphene Composite as Anode Materials for Lithium Ion Batteries. *J. Electroanal. Chem.* **2015**, *739*, 36−42.